Talanta 107 (2013) 211–218

Contents lists available at SciVerse ScienceDirect

Talanta

journal homepage: www.elsevier.com/locate/talanta

Electrochemical sensor for bisphenol A based on magnetic nanoparticles decorated reduced graphene oxide

Yixuan Zhang [a], Yuxiao Cheng [b], Yuyan Zhou [b], Bingyu Li [a], Wei Gu [a], Xinhao Shi [a], Yuezhong Xian [a,*]

[a] Department of Chemistry, East China Normal University, Shanghai 200062, China
[b] Shanghai Entry–Exit Inspection and Quarantine Bureau, Shanghai 200135, China

ARTICLE INFO

Article history:
Received 15 November 2012
Received in revised form
7 January 2013
Accepted 9 January 2013
Available online 17 January 2013

Keywords:
Bisphenol A
Magnetic nanoparticles
Reduced graphene oxide
Electrochemical sensor

ABSTRACT

Bisphenol A (BPA), as one kind of endocrine-disrupting chemicals, has adverse impact on human health and environment. It is urgent to develop effective and simple methods for quantitative determination of BPA. In this work, an electrochemical sensor for BPA based on magnetic nanoparticles (MNPs)-reduced graphene oxide (rGO) composites and chitosan was presented for the first time. The MNPs-rGO composites were characterized by scanning electron microscopy, X-Ray diffraction and Fourier transform infrared spectroscopy. Electrochemical studies show that MNPs-rGO composites can lower the oxidation overpotential and enhance electrochemical response of BPA due to the synergetic effects of MNPs and rGO. Under the optimal experiment conditions, the oxidation peak current was proportional to the concentration of BPA over the range of 6.0×10^{-8} to 1.1×10^{-5} mol L^{-1} with the detection limit of 1.7×10^{-8} mol L^{-1}. Moreover, the MNPs-rGO based electrochemical sensor shows excellent stability, reproducibility and selectivity. The electrochemical sensor has been successfully applied to the determination of BPA in real samples with satisfactory results.

1. Introduction

Bisphenol A ($(CH_3)_2C(C_6H_4OH)_2$, BPA) is a key monomer in the industrial production for polycarbonate polymers [1], epoxy resins [2], along with other materials to make plastics, which have been widely used as plastic food containers, food can linings and water bottles, and so on [3]. As an additive in plastics manufacturing process, BPA could make products with colorless, transparent, durable, lightweight and prominent anti-impact properties [4]. However, BPA is one kind of endocrine-disrupting chemicals which can mimic estrogen and lead to negative health effects on animals and human beings [5]. BPA exhibits endocrine disruption in binding to estrogen receptors, such as alterations in endogenous hormone synthesis, hormone metabolism and hormone concentrations in blood [6]. These disruptions can cause cancerous tumors, birth defects and other developmental disorders even at very low part-per-trillion doses [7]. BPA not only has a negative impact on human health, but also on environment. Several reports indicate that BPA can migrate into environment through the manufacturing process of plastics and the degradation process of waste plastics [8]. Therefore, it is urgent to develop a simple and fast method to determine BPA for protection of environment and health.

At present, some methods have been established for determination of BPA. Chromatographic technique, for example, gas chromatography coupled with mass spectrometry [9] and high-performance liquid chromatography equipped with ultra-violet, fluorescence, mass spectrometry and electrochemical detection [10] have been developed for BPA measurement. Chromatographic technique exhibits high sensitivity and good precision, however, it needs quite expensive and complicated instruments, time-consuming pretreatment steps and skilled operators. Thus, chromatographic technique is not suitable for fast and on-site measurement. Some other methods, such as enzyme linked immunosorbent assays [11], molecular imprinting technique [12], flow injection inhibitory chemiluminescence method [13], quartz crystal microbalance sensor [14], impedimetric immunosensor [15], capacitive sensor [16], fluorescence sensor [17] and electrochemical sensor have been developed for BPA determination. Among these strategies, electrochemical methods have attracted wide attentions because of fast response, cheap instrument, low cost, easy preparation, high sensitivity, excellent selectivity and real-time detection. In order to enhance the electrochemical response of BPA, different electrode materials have been developed to improve the sensitivity and selectivity of the electrochemical sensors. Molecularly imprinted polymer [18], metallophthalocyanine polymer [19], thionine [20], metal nanoparticle based composites [21] and carbon based materials [22–25] have been reported to be used as electrode matrix for BPA determination. Graphene, as a novel one-atom-thick carbon

* Corresponding author. Tel.: +86 21 5434 0048.
E-mail address: yzxian@chem.ecnu.edu.cn (Y. Xian).

0039-9140/$ - see front matter © 2013 Elsevier B.V. All rights reserved.
http://dx.doi.org/10.1016/j.talanta.2013.01.012

material, has received a great deal of attention in fundamental and applied research since it has been discovered in 2004 [26]. It has been used as novel electrode matrix because of its large surface area, high mechanical strength, fast electron transfer rate, excellent thermal and electrical conductivity [27]. Graphene and its derivatives have been used to develop electrochemical sensors for BPA determination. Nitrogen-doped graphene sheets were used as electrode matrix by Fan and coworkers to fabricate an electrochemical sensor for BPA measurement [28]. Ntsendwana et al. reported an electrochemical sensor for BPA by modified glassy carbon electrode (GCE) with graphene via a simple drop and dry method [29]. Voltammetric detection of BPA was developed by Wang and colleagues with a chitosan (CS)–graphene composite modified carbon ionic liquid electrode [30]. Au–Pd alloy nanoparticles/graphene composite was prepared by Huang et al. and the nanocomposites were successfully used as electrode matrix for BPA detection [31].

In recent years, magnetic nanoparticles (MNPs) have been attracting much interest in the fields of advanced biological and medical applications as well as in the fields of separation science [32]. Very recently, magnetic materials coated with molecularly imprinted polymer were used as solid-phase extraction adsorbent to removal BPA because of their large surface area and superparamagnetism [33–35]. MNPs based composites were applied to electrochemical detection of BPA [36–38]. In this work, Fe_3O_4 nanoparticles decorated reduced graphene oxide (rGO) were synthesized by in situ chemical coprecipitation of Fe^{2+} and Fe^{3+} in alkaline solution in the presence of rGO. Due to the synergetic effects of MNPs and rGO, the composites of MNPs-rGO exhibit remarkable potential as electrode matrix for enrichment and determination of BPA. It is found that MNPs-rGO modified electrode can lower the oxidation overpotential of BPA and improve the sensitivity for BPA determination.

2. Experimental

2.1. Reagents and materials

Natural graphite (99.95% pure), ferric chloride hexahydrate ($FeCl_3 \cdot 6H_2O$), ferrous chloride tetrahydrate ($FeCl_2 \cdot 4H_2O$), sodium hydroxide, chitosan were purchased from Sinopharm Chemical Reagent Company. BPA was purchased from TCI (Shanghai) and its stock solution (0.1 mol L^{-1}) was prepared with ethanol. The working solutions were prepared by diluting the stock solution with phosphate buffer solution (PBS, 0.2 mol L^{-1}, pH 8.0). All the chemicals were used directly without further purification. All other chemicals and solvents were of analytical grade. Ultrapure water was used throughout the experiments.

2.2. Apparatus and measurements

Surface morphological images of rGO and MNPs-rGO were recorded by a HITACHI S-4800 scanning electronic microscope (SEM) (Hitachi, Japan). X-Ray powder diffraction (XRD) measurements were performed on a powder sample of rGO and MNPs-rGO using a Rigaku D/Ultima IV X-ray diffractometer (Rigaku, JAPAN), which was operated at 35 kV and 40 mA at a scan rate of $0.4^{\circ}s^{-1}$ using Cu-Kα radiation ($\lambda = 0.1542$ nm). Fourier transform infrared (FTIR) spectra were recorded on a NEXLIS FTIR (Nicolet, USA) and samples were dried at 90 °C vacuum for at least 3 h prior to fabrication of the KBr pellet.

All electrochemical experiments were performed with a computer-controlled Autolab (TYPE III, Netherlands) electrochemical workstation with a conventional three-electrode cell. A bare GCE (diameter, 3 mm) or modified GCE was used as working electrode. A saturated calomel electrode (SCE) and a platinum wire were used as reference electrode and auxiliary electrode, respectively. All solutions were deoxygenated by bubbling pure nitrogen for at least 10 min. The modified electrode was treated in the blank PBS before each measurement by successive cyclic voltammetric sweeps until the steady curve appeared.

2.3. Synthesis of MNPs-rGO

GO was synthesized according to the modified Hummer's method [39]. Then, rGO was obtained by reducing GO with hydrazine hydrate. Briefly, GO (100 mg) was dispersed in 200 mL water to create a 0.05 wt% of dispersion. Prior to reduction, the dispersion was ultrasonicated for 3 h using an ultrasonic cleaner (180 W, 40 Hz), in which the bulk GO powders were transformed into GO sheets. The obtained brown dispersion was concentrated at 3000 rpm for 30 min to remove any un-exfoliated GO. Then, 200 μL of hydrazine hydrate and 3 mL of ammonia solution were added to GO solution. After that, the mixture was stirred vigorously for a few minutes and refluxed at 80 °C for 12 h in an oil bath. The final products were then centrifuged, washed with water, and finally dried under vacuum.

MNPs-rGO composites were synthesized by in situ chemical coprecipitation of Fe^{2+} and Fe^{3+} in alkaline solution in the presence of rGO. The molar ratio of Fe^{2+} and Fe^{3+} was 1:2. Firstly, 200 mg rGO, 344.4 mg $FeCl_2 \cdot 4H_2O$ (1.732 mmol) and 561.9 mg $FeCl_3$ (3.464 mmol) were dissolved in 200 mL of deionized water. Then, 1.5 mL NaOH (10 mol L^{-1}) solution was added and the pH of the solution was controlled to be in the range of 11–12. After that, the mixture was heated to 80 °C under continuous mechanical stirring for 1 h. The precipitate was separated by a permanent magnet and washed with double distilled water. The obtained materials were dried under vacuum at 60 °C.

2.4. Preparation of electrochemical sensor

Prior to use, the GCE was polished with 0.3 and 0.05 μm alumina powder, respectively. After cleaned ultrasonically in ethanol and doubly distilled water successively, the GCE was dried at room temperature. CS was chosen to immobilize different materials on GCE due to its excellent biocompatibility and film-forming ability. For preparation of the modified electrode, 1.5 mg L^{-1} MNPs-rGO was mixed with CS by ultrasonication for 1 h to obtain a homogeneously dispersed solution. Then, 5.0 μL mixtures were dropped on the surface of the GCE and dried under IR lamp. After that, the electrode surface was thoroughly rinsed with doubly distilled water and dried under ambient condition. The obtained electrode was denoted as CS/MNPs-rGO/GCE. As for comparison, CS modified GCE (CS/GCE), Fe_3O_4 nanoparticles and CS mixture modified GCE (CS/MNPs/GCE), rGO and CS modified GCE (CS/rGO/GCE) were fabricated with similar procedures.

3. Results and discussion

3.1. Material characterization

The morphologies of rGO and MNPs-rGO hybrid material were investigated by SEM. As shown in Fig. 1(A), rGO displays a wrinkled paper-like structure. From Fig. 1(B), it could be seen that some white spots, which are MNPs, are uniformly deposited on the surface of the rGO. The average size of the nanoparticles estimated from SEM observation is about 12 nm. Some nanoparticles are slightly aggregated due to the close to saturation loading degree [40]. It is worth noting that MNPs could serve as stabilizer to separate rGO sheets against aggregation [41], hence,

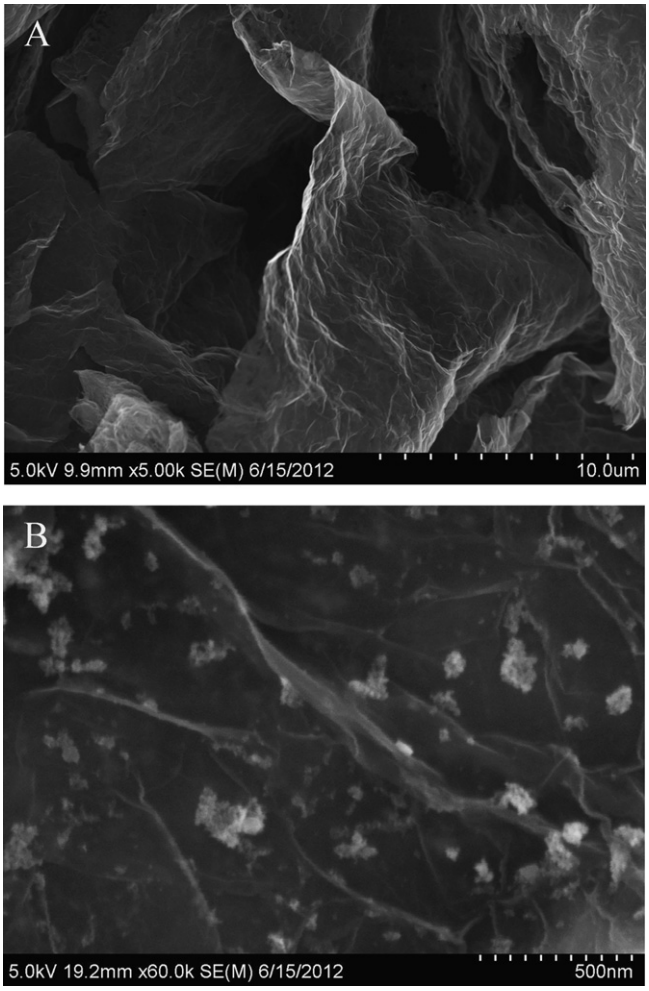

Fig. 1. SEM images of rGO (A) and MNPs-rGO (B).

the paper-like structure can be observed clearly while rGO decorated with Fe_3O_4 nanoparticles.

XRD measurements were carried out to investigate the phase and structure of the obtained samples. The patterns of GO, rGO, and MNPs-rGO are shown in Fig. 2. The pattern of GO shows a peak at $2\theta=10.4^\circ$, indicating that the AB stacking order is still observed in GO [42]. While GO is reduced by hydrazine hydrate, a broad peak at $2\theta=26.5^\circ$ appears, which corresponds to the (002) reflection of rGO [42]. The (002) reflection is very broad, indicating that free graphene sheets are very poorly ordered along the stacking direction [43]. As for MNPs-rGO, the peaks at 2θ of 18.1°, 30.3°, 35.7°, 43.5°, 53.5°, 57.5° and 62.9° can be assigned to (111), (220), (311), (400), (422), (511) and (440) of crystal planes of Fe_3O_4 (JCPDS No. 75-0033). Besides these peaks, the additional peak at 26.5° for the (002) reflection of rGO demonstrates the coexistence of MNPs and rGO in the composites. The crystallite size of Fe_3O_4 nanoparticles on rGO sheets is calculated from the full-width at half maximum of the strongest reflection of the (311) using the Debye–Scherrer equation,

$$D=\frac{K\lambda}{\beta\cos\theta}$$

where D is the average particle size (nm) of the samples, λ is the wavelength of Cu-K_α (0.1541 nm), K is the constant, θ and β are the Bragg angle and full width at half maximum (radians), respectively. In this work, the average particle size for magnetic Fe_3O_4 nanoparticles is about 13 nm, which is in good agreement with the observation of SEM.

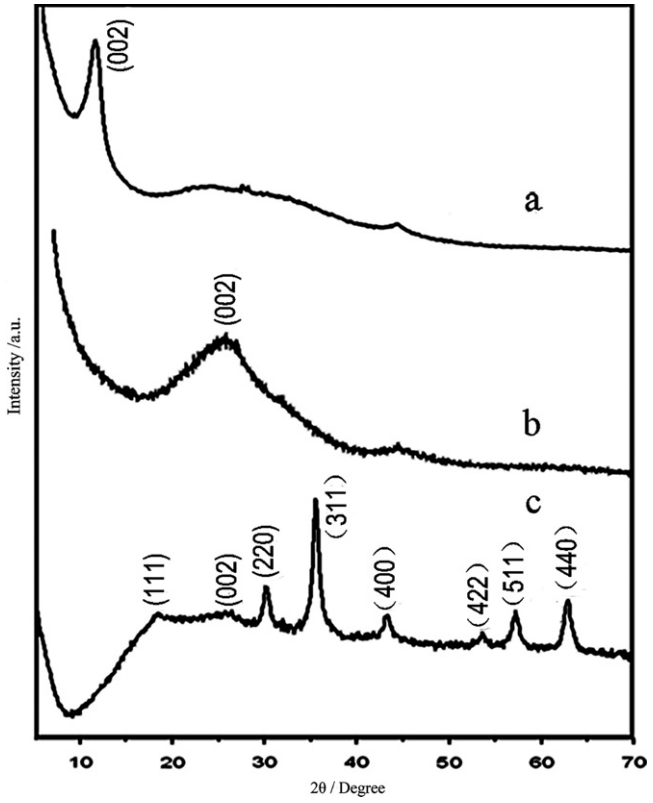

Fig. 2. XRD patterns of GO (a), rGO (b) and MNPs-rGO (c).

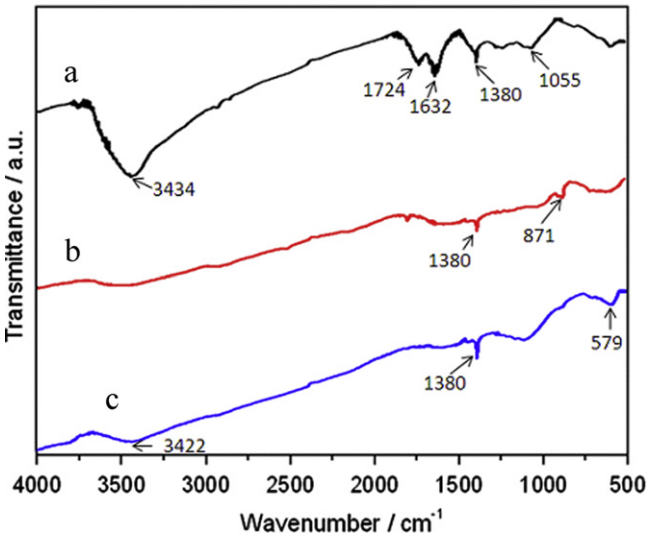

Fig. 3. FTIR spectra of GO (a), rGO (b) and MNPs-rGO (c).

Fig. 3 shows the FTIR spectra of GO, rGO and MNPs-rGO composites. As for GO, the characteristic peaks at 1055, 1380 and 1724 cm^{-1} are corresponding to the vibration of alkoxy (C–O), carboxyl (C–OH) and carbonyl (C=O), respectively [44]. The peak located at 1632 cm^{-1} assigns to the C=C skeletal vibrations of unoxidized graphitic domains or the deformation vibration of intercalated water molecule [45]. The broad band at 3424 cm^{-1} could be due to the O–H stretching [46]. After GO is reduced, the characteristic adsorption bands of oxygen-containing groups almost disappear. Only the low intensity peak at 1380 cm^{-1} for C–OH remains, which is due to the residual surface oxygen species that are not completely removed [47]. The peaks at

871 cm^{-1} may be assigned to the skeletal vibration of C–C. In comparison with the FTIR spectrum of rGO, the MNPs-rGO shows a characteristic band at 579 cm^{-1}, implying the lattice absorption of iron oxide [48].

3.2. Electrochemical characterizations

Electrochemical behaviors of the different electrodes were investigated using $K_3[Fe(CN)_6]$ as redox probes. Fig. 4 shows the cyclic voltammograms (CVs) of different electrodes in the aqueous solution of 5.0 mmol L^{-1} $K_3[Fe(CN)_6]$ containing 0.1 mol L^{-1} KCl at a scan rate of 100 mV s^{-1}. At bare GCE (Fig. 4a), a couple of redox peaks appear with a peak-to-peak separation (ΔE_p) of 98 mV. As for CS/MNPs/GCE, CS/rGO/GCE and CS/MNPs-rGO/GCE, ΔE_p is about 72 mV, 81 and 93 mV, respectively. It indicates relatively fast electron transfer at modified electrodes. Compared with bare GCE, the redox currents of $K_3[Fe(CN)_6]$ at CS/MNPs/GCE is increased (Fig. 4c). It is most likely related to the excellent electrical conductivity and the large surface area of MNPs on the electrode surface. As for CS/rGO/GCE (Fig. 4d), the current densities are higher than that of CS/MNPs/GCE, indicating that rGO could accelerate the electron transfer rate. Moreover, the peak current increases continuously while MNPs are introduced on rGO (Fig. 4e). It indicates that MNPs play important role in the increase of the electroactive surface area. Only at CS modified electrode, the redox peak current is lower than that of bare GCE due to the electro-inactivity of CS (Fig. 4b).

For further characterization of the modified electrodes, the electrochemical impedance spectroscopy (EIS) was used in the frequency range from 0.1 to 10^4 Hz at the formal potential of 0.18 V. Fig. 5 shows Nyquist diagrams of different electrodes in 5.0 mmol L^{-1} $[Fe(CN)_6]^{3-/4-}$ solution containing 0.1 mol L^{-1} KCl. It can be seen that a well-defined semicircle at higher frequencies is obtained at the bare GCE (Fig. 5a) and the electron transfer resistance (R_{ct}) value is about 125.1 Ω. As for CS/GCE (Fig. 5b), the R_{ct} value is ca. 210.3 Ω, indicating that the CS film on GCE hinders the electron transfer between the redox probe of $[Fe(CN)_6]^{3-/4-}$ and the electrode surface. The R_{ct} value decreases dramatically while the bare electrode is modified with MNPs and CS (Fig. 5c). Compared with bare GCE, the R_{ct} of CS/MNPs/GCE greatly decreases to 25.1 Ω, implying that MNPs can greatly improve the conductivity and the electron transfer process. While rGO and CS (Fig. 5d) is deposited on GCE, the Nyquist plot shows almost line portion with the R_{ct} value of about 10.9 Ω. After coated with CS/MNPs-rGO (Fig. 5e), the R_{ct} value decreases to 7.9 Ω. It is possibly due to the good conductivity and the large surface area of MNPs-rGO composites.

3.3. Electrochemical behaviors of BPA

Electrochemical behaviors of different electrodes in the absence and presence of 0.1 mM BPA were investigated by cyclic voltammetry at the scan rate of 100 mV s^{-1}. No redox peak is observed at each electrode without BPA. Fig. 6 shows the electrochemical responses of 0.1 mM BPA at different electrodes. At bare GCE, a relatively small oxidation peak with the potential of 0.52 V and the peak current about 4.93 μA is observed (Fig. 6a). After coated with CS, the oxidation current increases a little due to the electrostatic adsorption (Fig. 6b). As shown in Fig. 6c, the peak current of BPA increases distinctly, indicating MNPs can electrocatalytically oxidize BPA. After introducing rGO onto GCE, the back-ground currents increase due to the high capacitance for the sp^2-hybridized structure of graphene [49]. It can be seen that the peak current increases continuously at the CS/rGO/GCE (Fig. 6d), which reveals that rGO acts as an effective electron promoter for electrocatalytic oxidation of BPA. The electrochemical response of BPA at CS/MNPs-rGO/GCE (Fig. 6e) is bigger than

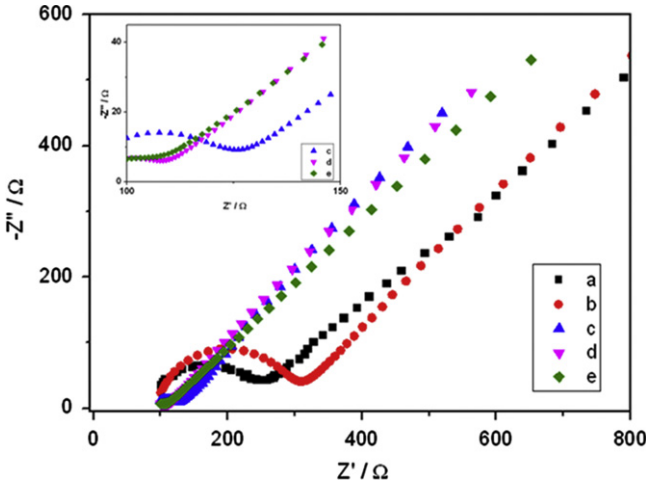

Fig. 5. Nyquist plots of bare GCE (a), CS/GCE (b), CS/MNPs/GCE (c), CS/rGO/GCE (d) and CS/MNPs-rGO/GCE (e) in 5.0 mM $K_3[Fe(CN)_6]$ containing 0.1 M KCl. The frequency varies from 0.1 to 10^4 Hz at the formal potential of 0.18 V. Inset is the magnified plots of (c), (d) and (e) at the high-frequency region.

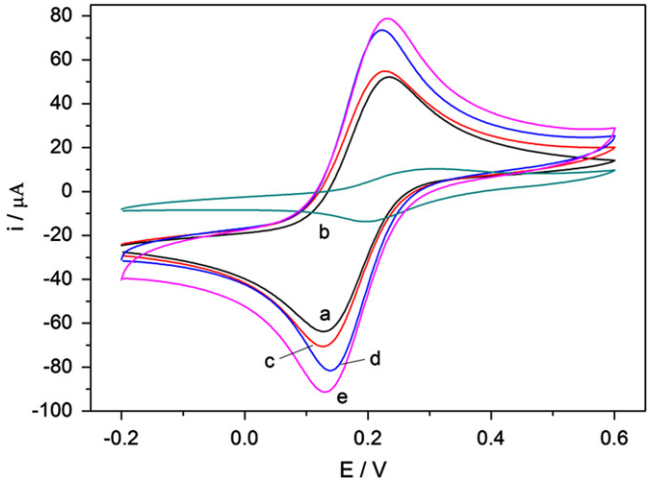

Fig. 4. CVs of bare GCE (a), CS/GCE (b), CS/MNPs/GCE (c), CS/rGO/GCE (d) and CS/MNPs-rGO/GCE (e) in 5.0 mM $K_3[Fe(CN)_6]$ containing 0.1 M KCl. (υ=100 mV s^{-1}).

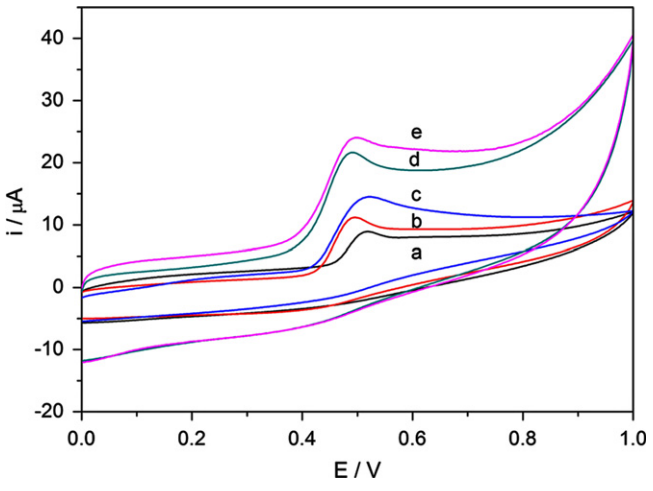

Fig. 6. CVs of bare GCE (a), CS/GCE (b), CS/MNPs/GCE (c), CS/rGO/GCE (d) and CS/MNPs-rGO/GCE (e) in 0.2 M PBS (pH 8.0) containing 0.1 mM BPA. (υ=100 mV s^{-1})

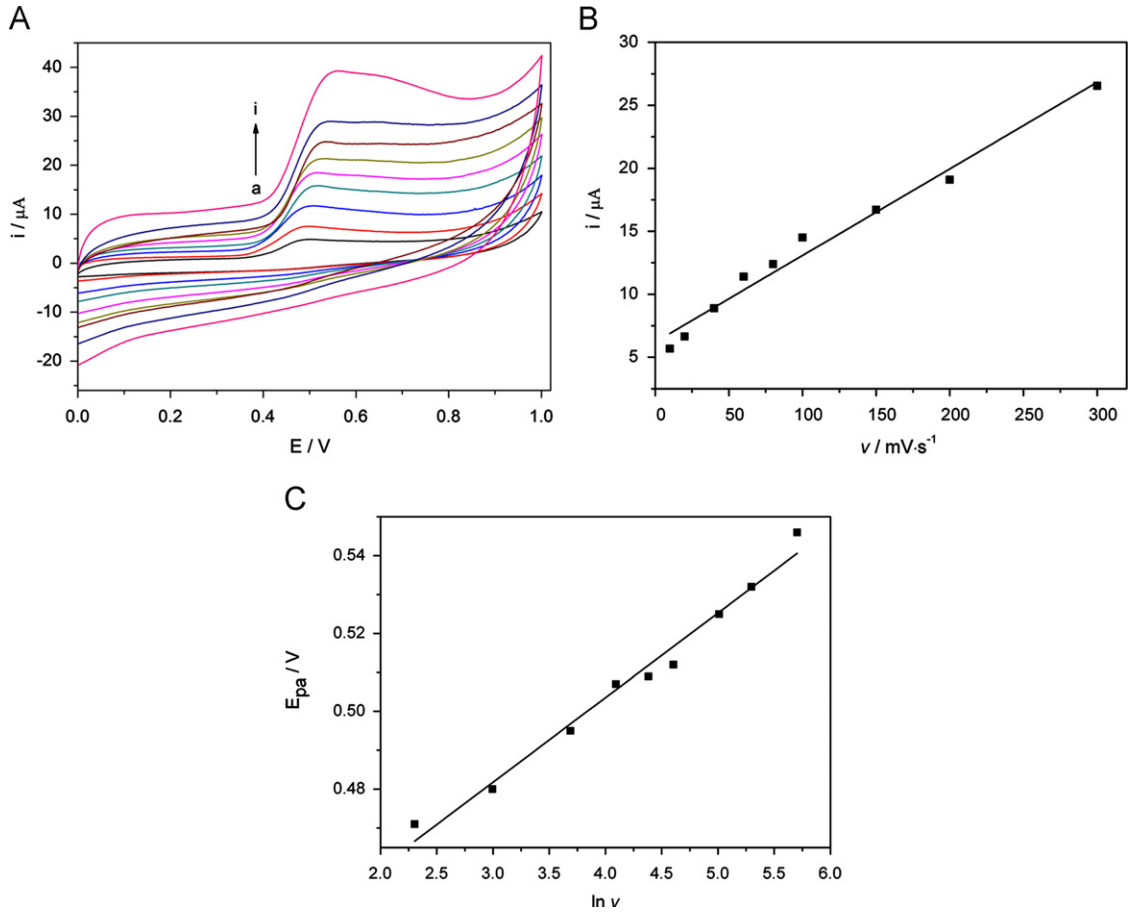

Fig. 7. (A) Cyclic voltammograms of 0.1 mM BPA at CS/MNPs-rGO/GCE with different scan rates. Curves (a–i) are obtained at 10, 20, 40, 60, 80, 100, 150, 200, 300 mV s^{-1}, respectively. (B) Dependence of the oxidation peak current on the scan rate. (C) The relationship between E_{pa} and ln v.

that at CS/rGO/GCE under the same experimental conditions, indicating the synergistic effect between MNPs and rGO. In addition, the peak current increases dramatically to 15.04 μA by subtracting the back-ground currents. Moreover, the experimental data also show that MNPs-rGO composites can enhance the electron transfer rate and lower the overpotential of BPA oxidation. As shown in Fig. 6(e), the oxidation potential of BPA at CS/MNPs-rGO/GCE is about 0.49 V, which is lower than that of bare GCE (0.52 V).

Electrochemical behaviors of BPA at CS/MNPs-rGO/GCE with different scan rates are further investigated. From Fig.7A, it can be seen that the oxidation peak currents increase linearly with scan rate in the range from 10 to 300 mV s^{-1}. The regression equation can be expressed as I_{pa} (μA)=0.0688v (mV s^{-1})+6.2049 (R=0.99), indicating the oxidation of BPA at CS/MNPs-rGO/GCE is an adsorption-controlled electrode process (Fig. 7B). Moreover, a linear correlation of E_{pa} versus ln v is observed and it follows the equation of E_{pa} (V)=0.022 ln v+0.4165 (R=0.99) (Fig. 7C). As for an adsorption-controlled and totally irreversible electrode process, E_{pa} is defined by the following equation [50],

$$E_{pa} = E^0 + \left(\frac{RT}{\alpha nF}\right)\ln\left(\frac{RT\,K^0}{\alpha nF}\right) + \left(\frac{RT}{\alpha nF}\right)\ln v$$

where α is transfer coefficient, K^0 is standard rate constant of the reaction, n is electron transfer number involved in rate-determining step, v is scan rate, E^0 is formal redox potential, and R, T, F have their usual meanings. According to the slope of the plot of E_{pa} versus ln v, the value of αn is calculated to be 1.16. Generally, α is assumed to be 0.5 in totally irreversible electrode process.

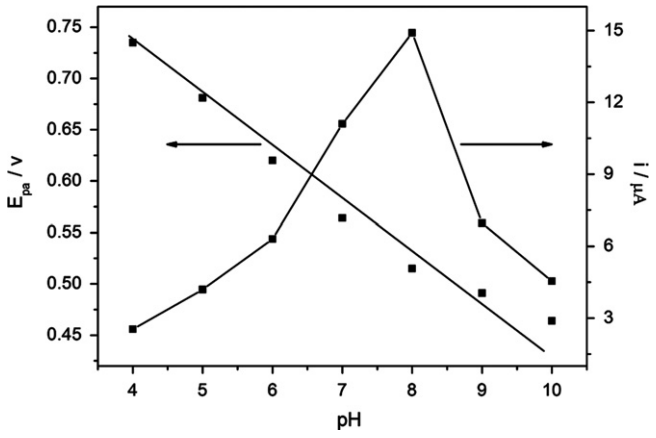

Fig. 8. Effects of pH on the peak current and oxidation potential of BPA at CS/MNPs-rGO/GCE.

Thus, the electron transfer number (n) for oxidation of BPA is around 2.

3.4. Optimization of experimental conditions

The effect of pH on the electrochemical responses of BPA at CS/MNPs-rGO/GCE was studied over the pH ranging from 3.0 to 10.0 (Fig. 8). The oxidation currents increase gradually over the pH range from 3.0 to 8.0. While the pH value exceeds 8.0, the oxidation current decreases. Therefore, PBS with the pH value of 8.0 was chosen as the supporting electrolyte. At the same time,

the peak potential shifts negatively along with the increase of pH value. The relationship between the E_{pa} and pH is shown in Fig. 8, and it obeys the following equation,

$E_{pa}(V) = -0.0524\ pH + 0.993\ (R = 0.9917)$.

A slope of about -52.4 mV per pH unit is close to the theoretical value of 57.6 mV pH^{-1}. It indicates that the electron transfer of this electrochemical reaction is accompanied by an equal number of electrons and protons. Based on the result that the electron transfer number (n) for oxidation of BPA is around 2, the electrooxidation of BPA at CS/MNPs-rGO/GCE is a two-electron and two-proton process.

The concentration of MNPs-rGO suspension on the electrode surface plays an important role for BPA oxidation. In our experiment, the concentration of CS was fixed at 1.5 mg L^{-1} and the volume of the different suspensions casted onto the GCE surface was controlled to be 5.0 μL. With increasing concentration of MNPs-rGO from 0.25 to 1.5 mg L^{-1} (Fig. 9), the peak currents increase obviously. It might ascribe to the expansion of the conductive electrode area and the increase of accumulation ability. Further increase of the concentration of MNPs-rGO leads to a decrease in the peak current, which is probably attributed to the limited mass transport of BPA inside a thicker film. Hence, a concentration of 1.5 mg L^{-1} MNPs-rGO was chosen to modify GCE for the electrochemical detection of BPA.

3.5. Differential pulse voltammetric determination

Accumulation can improve the amount of BPA adsorbed on the electrode surface, and then enhance the determination sensitivity and lower the detection limit. Therefore, the effects of accumulation potential and time on the electrochemical responses of BPA were further investigated. While the accumulation potential is varied from -0.30 to 0.30 V, the oxidation peak currents of 0.1 mM BPA in PBS do not change obviously, implying that the accumulation process is almost independent of the accumulation potential. On the other hand, the oxidation peak current increases gradually with the accumulation time up to 60 s. It suggests that more BPA could be adsorbed on the electrode surface with extending accumulation time. As the accumulation time increases, the peak current levels off, illustrating that the adsorptive equilibrium is reached. Therefore, the optimum accumulation time for BPA was selected as 60 s.

Differential pulse voltammetry (DPV) with high sensitivity was used to evaluate the analytical performance of the electrochemical sensor (Fig. 10). BPA was added to 10 mL PBS buffer (pH 8.0) successively under magnetic stirring. Under the optimal experimental conditions, a linear relationship between oxidation current and BPA concentration is obtained over the range of 6.0×10^{-8}–1.1×10^{-5} mol L^{-1}, and the regression equation could be expressed as i(μA)=0.0181c (μM)+0.01 with the correlation coefficient of 0.9977. The limit of detection (LOD) is estimated to be 1.7×10^{-8} mol L^{-1} at a ratio of signal to noise of 3. Compared with other works (as shown in Table 1), the analytical performance of the electrochemical sensor based on MNPs-rGO composites is very well.

3.6. Reproducibility, stability and selectivity of CS/MNPs-rGO/GCE

In order to investigate the reproducibility, five CS/MNPs-rGO modified electrodes were fabricated by the same procedure. Then cyclic voltammetric responses of 0.1 mM BPA at CS/MNPs-rGO modified electrodes were recorded. The relative standard deviation (RSD) for the oxidation peak currents with six determinations is 2.69%, indicating excellent reproducibility of the modified electrode. The stability of CS/MNPs-rGO/GCE was checked over a period of two weeks. After two weeks, the peak current of 0.1 mM BPA retained 92.3% of the initial response. In order to evaluate the selectivity of the electrochemical sensor, the influence of some possible substances were examined in pH 8.0 PBS buffer containing 10 μM BPA. The results show that 50-fold concentration of dimethyl phthalate, benzene, naphthalene, p-nitroaniline, ethanol, acetonitrile had no obvious influence on the electrochemical response of BPA with deviations below 5.0%. Otherwise, some metal ions such as 100-fold concentration of Na^+, Mg^{2+}, Al^{3+}, Zn^{2+}, Fe^{3+}, Cu^{2+}, Pb^{2+}, Cd^{2+} did not interfere the determination of BPA. It was worth noting that phenolic chemicals such as phenol, naphthol could interfere with the detection of BPA. However, this interference has no influence on the practical application, because phenolic chemicals except BPA are not commonly used in the production of plastics [55].

3.7. Practical application

In order to evaluate the performance of CS/MNPs-rGO/GCE in practical analytical application, the determination of BPA in the real samples was carried out through a recovery study according to the above-described analytical procedure. In brief, different kinds of plastic products were cut into small pieces, then grinded into a powder using liquid nitrogen frozen grinder. After that,

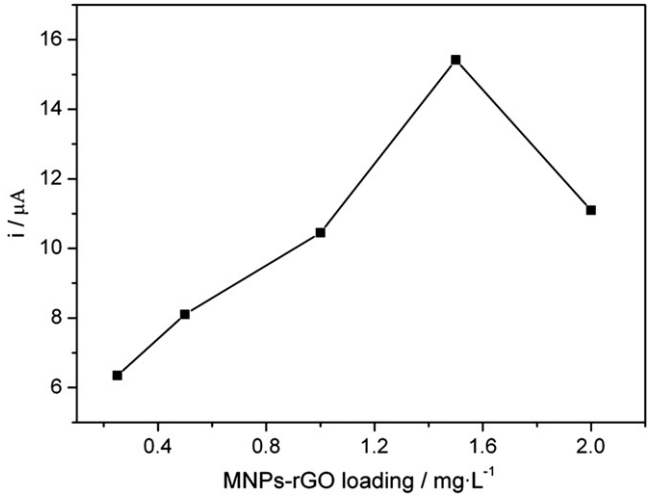

Fig. 9. Effect of the amount of MNPs-rGO on the electrochemical response of 0.1 mM BPA.

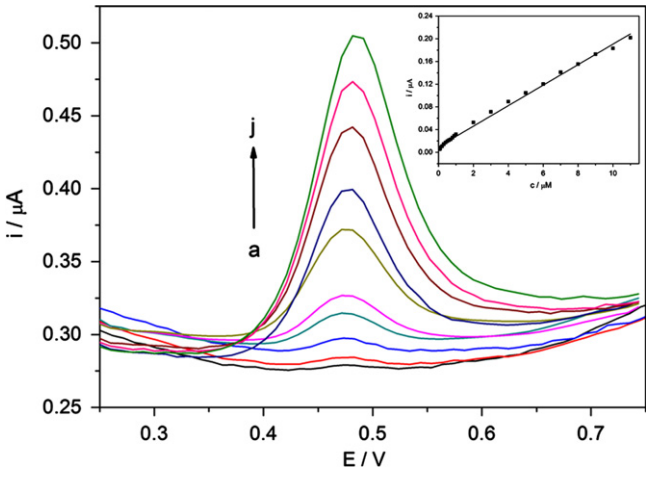

Fig. 10. Differential pulse voltammograms for BPA with different concentrations of BPA (from a to j: 0.06, 0.09, 0.2, 0.6, 1, 3, 5, 7, 9, 11 μM). Insert is the relationship between the oxidation peak current and the concentration of BPA.

Table 1
Comparison the performance of the CS/MNPs-rGO/GCE for BPA detection with other sensors.

Sensors	Linear range ($\mu mol\ L^{-1}$)	LOD ($\mu mol\ L^{-1}$)	References
Tyr[a]-SF[b]-MWNTs[c]-CoPc[d]/GCE	0.05–3.0	0.03	[22]
MWCNT-GNPs[e]/GCE	0.02–20	0.0075	[23]
Graphene/GCE	0.05–1	0.04689	[29]
Chistosan-graphene/CILE[f]	0.1–800	0.0264	[31]
CS[g]-Fe_3O_4/GCE	0.05–30	0.008	[38]
CNT[h]/GCE	0.3–100	0.098	[51]
SWNT[i]-tyrosinase/CPE[j]	0.1–12	0.02	[52]
MCM-41/CPE	0.22–8.8	0.038	[53]
Boron-doped diamond electrode	0.44–5.2	0.21	[54]
Tyr-nanographene/GCE	0.1–2	0.033	[55]
CS/MNPs-rGO/GCE	0.06–11	0.0167	This work

[a] Tyr: tyrosinase.
[b] SF: silk fibroin.
[c] MWNTs : multiwalled carbon nanotubes.
[d] CoPc :cobalt phthalocyanine.
[e] GNPs :gold nanoparticles.
[f] CILE: carbon ionic liquid electrode.
[g] CS: chitosan.
[h] CNT: carbon nanotube.
[i] SWNT : single walled carbon nanotube.
[j] CPE: carbon paste electrode.

Table 2
Determination of BPA in plastic samples by CS/ MNPs-rGO/GCE.

Sample	Measured[a] (μM)	Added(μM)	Found[a] (μM)	RSD (%)	Recovery (%)
PC[b] drinking bottle	0.82	1.00	1.77	4.69	97.3
PC[b] ice bucket	0.77	3.00	4.13	0.94	109.2
PS[c] condiment box	Not detected	1.00	0.97	2.06	97.0
PP[d] water glass	Not detected	1.00	1.09	3.16	109.0
PET[e] snack box	Not detected	1.00	1.08	2.56	108.0
PS[c] fruit dish	Not detected	5.00	5.19	4.89	103.8

[a] $n=3$.
[b] PC: Polycarbonate.
[c] PS: Polystyrene.
[d] PP: Polypropylene.
[e] PET: Poly(Ethylene Terephthalare).

about 1.00 g of plastic powder was added into 20 mL methanol, then extracted by ultrasonic. After filtrated, the liquid phase was concentrated by pressure blowing concentrator. Under the optimal experimental conditions, a known-amount of sample solution was added into PBS (pH8.0) and analyzed by DPV. The results are shown in Table 2. Only polycarbonate sample contains BPA. No BPA is detected in the other samples, such as polystyrene, polypropylene and poly(ethylene terephthalate). Moreover, it can be seen that the recovery is over the range from 97.0% to 109.2%, indicating that the proposed procedure is reliable, effective and accurate for practical applications.

4. Conclusions

In this work, MNPs-rGO composites have been successfully synthesized. Owing to the adsorption capacity and electrochemical conductivity, MNPs-rGO composites are used as new electrode matrix for BPA measurement. The electrochemical sensor based on MNPs-rGO composites displays an electrocatalytic performance to the oxidation of BPA with broad linear range and low detection limit. Moreover, the electrochemical sensor shows good sensitivity, selectivity and reproducibility. The CS/MNPs-rGO/GCE is proved to be an accurate and reliable method due to the determination of BPA in real samples with satisfactory results. Furthermore, the CS/MNPs-rGO/GCE shows a potential application prospect for on-site measurement of BPA with simple preparation and low cost.

Acknowledgments

This work was supported by the National Natural Science Foundation of China (No. 21175046), New Century Excellent Talents in University (No. NCET-09–0357) and General Administration of Quality Supervision, Inspection and Quarantine of China (Nos. 2011IK041 and 2012IK048)

References

[1] C.F. Abrams, K. Kremer, Macromolecules 36 (2003) 260–267.
[2] S. Ahmada, A.P. Guptab, E. Sharmina, M. Alama, S.K. Pandey, Prog. Org. Coat 54 (2005) 248–255.
[3] C. Brede, P. Fjeldal, I. Skjevrak, H. Herikstad, Food Addit. Contam 20 (2003) 684–689.
[4] K. Marsh, B. Bugusu, J. Food Sci. 72 (2007) 39–55.
[5] W.V. Welshons, K.A. Thayer, B.M. Judy, J.A. Taylor, E.M. Curran, F.S. vom Saal, Environ. Health Perspect. 111 (2003) 994–1006.
[6] J.B. Matthews, K. Twomey, T.R. Zacharewski, Chem. Res. Toxicol. 14 (2001) 149–157.
[7] L.N. Vandenberg, R. Hauser, M. Marcus, N. Olea, W.V. Welshons, Reprod. Toxicol. 24 (2007) 139–177.
[8] J. Sajiki, J. Yonekubo, Envrion. Int. 30 (2004) 145–150.
[9] G. Gatidou, N.S. Thomaidis, A.S. Stasinakis, T.D. Lekkas, J. Chromatogr. A 1138 (2007) 32–41.
[10] Y. Watabe, K. Hosoya, N. Tanaka, T. Kondo, M. Morita, T. Kubo, Anal. Bioanal. Chem 381 (2005) 1193–1198.
[11] A. Kim, C.R. Li, C.F. Jin, K.W. Lee, S.H. Lee, K.J. Shon, N.G. Park, D.K. Kim, S.W. Kang, Y.B. Shim, J.S. Park, Chemosphere 68 (2007) 1204–1209.
[12] W.H. Zhao, N. Sheng, R. Zhu, F.D. Wei, Z. Cai, M.J. Zhai, S.H. Du, Q. Hu, J. Hazard. Mater. 179 (2010) 223–229.
[13] S.H. Wang, X.T. Wei, L.Y. Du, H.S. Zhuang, Luminescence 20 (2005) 46–50.
[14] N. Tsuru, M. Kikuchi, H. Kawaguchi, S. Shiratori, Thin Solid Films 499 (2006) 380–385.
[15] M.A. Rahman, M.J.A. Shiddiky, J.S. Park, Y.B. Shim, Biosens. Bioelectron. 22 (2007) 2464–2470.
[16] B.K. Kang, J.H. Kim, S. Kim, K.H. Yoo, Appl. Phys. Lett. 98 (2011) 073703.
[17] X. Wang, H.L. Zeng, L.X. Zhao, J.M. Lin, Anal. Chim. Acta 556 (2006) 313–318.
[18] Y.Q. Wang, Y.Y. Yang, L. Xu, J. Zhang, Electrochim. Acta 56 (2011) 2105–2109.
[19] V. Chauke, F. Matemadombo, T. Nyokong, J. Hazard. Mater. 178 (2010) 180–186.
[20] M. Portaccio, D. Di Tuoro, F. Arduini, M. Lepore, D.G. Mita, N. Diano, L. Mita, D. Moscone, Biosens. Bioelectron. 25 (2010) 2003–2008.
[21] H.S. Yin, Y.L. Zhou, S.Y. Ai, R.X. Han, T.T. Tang, L.H. Zhu, Microchim. Acta 170 (2010) 99–105.
[22] H.S. Yin, Y.L. Zhou, J. Xu, S.Y. Ai, L. Cui, L.S. Zhu, Anal. Chim. Acta 659 (2010) 144–150.
[23] X.M. Tu, L.S. Yan, X.B. Luo, S.L. Luo, Q.J. Xie, Electroanalysis 21 (2009) 2491–2494.
[24] Y. Gao, Y. Cao, D.G. Yang, X.J. Luo, Y.M. Tang, H.M. Li, J. Hazard. Mater 199–200 (2012) 111–118.
[25] H. Kuramitza, M. Matsushita, S. Tanaka, Water Res. 38 (2004) 2331–2338.
[26] K.S. Novoselov, A.K. Geim, S.V. Morozov, D. Jiang, Y. Zhang, S.V. Dubonos, I.V. Grigorieva, A.A. Firsov, Science 306 (2004) 666–669.
[27] D. Li, M.B. Müller, S. Gilje, R.B. Kaner, G.G. Wallace, Nat. Nanotech. 3 (2008) 101–105.
[28] H.X. Fan, Y. Li, D. Wu, H.M. Ma, K.X. Mao, D.W. Fan, B. Du, H. Li, Q. Wei, Anal. Chim. Acta 711 (2012) 24–28.
[29] B. Ntsendwana, B.B. Mamba, S. Sampath, O.A. Arotiba, Int. J. Electrochem. Sci. 7 (2012) 3501–3512.
[30] Q.X. Wang, Y.H. Wang, S.Y. Liu, L.H. Wang, F. Gao, F. Gao, W. Sun, Thin Solid Films 520 (2012) 4459–4464.
[31] C.X. Huang, Y.T. Wu, J.S. Chen, Z.Z. Han, J. Wang, H.B. Pan, M. Du, Electroanalysis 24 (2012) 1416–1423.
[32] S. Mornet, S. Vasseur, F. Grasset, E. Duguet, J. Mater. Chem. 14 (2004) 2161–2175.
[33] Z.K. Lin, W.J. Cheng, Y.Y. Li, Z.R. Liu, X.P. Chen, C.J. Huang, Anal. Chim. Acta 720 (2012) 71–76.
[34] Z. Xu, L. Ding, Y.J. Long, L.G. Xu, L.B. Wang, C.L. Xu, Anal. Methods 3 (2011) 1737–1744.
[35] J.Z. Liu, W.Z. Wang, Y.F. Xie, Y.Y. Huang, Y.L. Liu, X.J. Liu, R. Zhao, G.Q. Liu, Y. Chen, J. Mater. Chem. 21 (2011) 9232–9238.

[36] R.S.J. Alkasir, M. Ganesana, Y.H. Won, L. Stanciu, S. Andreescu, Biosens. Bioelectron. 26 (2010) 43–49.
[37] H.S. Yin, L. Cui, Q.P. Chen, W.J. Shi, S.Y. Ai, L.S. Zhu, L.N. Lu, Food Chem. 125 (2011) 1097–1103.
[38] C.M. Yu, L.L. Gou, X.H. Zhou, N. Bao, H.Y. Gu, Electrochim. Acta 56 (2011) 9056–9063.
[39] W.S.J. Hummers, R.E. Offeman, J. Am. Chem. Soc. 80 (1958) 1339–1339.
[40] W.N. Wang, Y.P. Li, Q.H. Wu, C. Wang, X.H. Zang, Z. Wang, Anal. Methods 4 (2012) 766–772.
[41] V. Chandra, J. Park, Y. Chun, J.W. Lee, I.C. Hwang, K.S. Kim, ACS Nano 4 (2010) 3979–3986.
[42] H.L. Guo, X.F. Wang, Q.Y. Qian, F.B. Wang, X.H. Xia, ACS Nano 3 (2009) 2653–2659.
[43] A.V. Murugan, T. Muraliganth, A. Manthiram, Chem. Mater. 21 (2009) 5004–5006.
[44] H. Jabeen, V. Chandra, S. Jung, J.W. Lee, K.S. Kim, S.B. Kim, Nanoscale 3 (2011) 3583–3585.
[45] T. Szabó, O. Berkesi, P. Forgó, K. Josepovits, Y. Sanakis, D. Petridis, I. Dékány, Chem. Mater. 18 (2006) 2740–2749.
[46] H.K. Jeong, Y.P. Lee, R.J.W.E. Lahaye, M.H. Park, K.H. An, I.J. Kim, C.W. Yang, C.Y. Park, R.S. Ruoff, Y.H. Lee, J. Am. Chem. Soc. 130 (2008) 1362–1366.
[47] M. Zhang, D.N. Le, Z.F. Du, X.M. Yin, L.B. Chen, Q.H. Li, Y.G. Wang, T.H. Wang, J. Mater. Chem. 21 (2011) 1673–1676.
[48] X.Y. Yang, X.Y. Zhang, Y.F. Ma, Y. Huang, Y.S. Wang, Y.S. Chen, J. Mater. Chem. 19 (2009) 2710–2714.
[49] D. Du, J. Liu, X.Y. Zhang, X.L. Cui, Y.H. Lin, J. Mater. Chem. 21 (2011) 8032–8037.
[50] E. Laviron, J. Electroanal. Chem. 52 (1974) 355–393.
[51] D. Vega, L. Agüí, A. González-Cortés, P. Yáñez-Sedeño, J.M. Pingarrón, Talanta 71 (2007) 1031–1038.
[52] D.G. Mita, A. Attanasio, F. Arduini, N. Diano, V. Grano, U. Bencivenga, S. Rossi, A. Aminee, D. Mosconec, Biosens. Bioelectron. 23 (2007) 60–65.
[53] F.R. Wang, J.Q. Yang, K.B. Wu, Anal. Chim. Acta 638 (2009) 23–28.
[54] G.F. Pereira, L.S. Andrade, R.C. Rocha-Filho, N. Bocchi, S.R. Biaggio, Electrochim. Acta 82 (2012) 3–8.
[55] L.D. Wu, D.H. Deng, J. Jin, X.B. Lu, J.P. Chen, Biosens. Bioelectron. 35 (2012) 193–199.